Nucleotide-Specific Recognition of Iron-Responsive Elements by Iron Regulatory Protein 1

Anna I. Selezneva, William E. Walden and Karl W. Volz

Department of Microbiology and Immunology, *University of Illinois at Chicago, Chicago, IL 60612-7334, USA*

Correspondence to Karl W. Volz: *kvolz@uic.edu*
http://dx.doi.org/10.1016/j.jmb.2013.06.023
Edited by Y. Yaniv

Abstract

IRP1 [*i*ron *r*egulatory *p*rotein (IRP) *1*] is a bifunctional protein with mutually exclusive end-states. In one mode of operation, IRP1 binds iron-responsive element (IRE) stem–loops in messenger RNAs encoding proteins of iron metabolism to control their rate of translation. In its other mode, IRP1 serves as cytoplasmic aconitase to correlate iron availability with the energy and oxidative stress status of the cell. IRP1/IRE binding occurs through two separate interfaces, which together contribute about two-dozen hydrogen bonds. Five amino acids make base-specific contacts and are expected to contribute significantly to binding affinity and specificity of this protein:RNA interaction. In this mutagenesis study, each of the five base-specific amino acids was changed to alter binding at each site. Analysis of IRE binding affinity and translational repression activity of the resulting IRP1 mutants showed that four of the five contact points contribute uniquely to the overall binding affinity of the IRP1:IRE interaction, while one site was found to be unimportant. The stronger-than-expected effect on binding affinity of mutations at Lys379 and Ser681, residues that make contact with the conserved nucleotides G16 and C8, respectively, identified them as particularly critical for providing specificity and stability to IRP1:IRE complex formation. We also show that even though the base-specific RNA-binding residues are not part of the aconitase active site, their substitutions can affect the aconitase activity of holo-IRP1, positively or negatively.

Introduction

Iron is an essential nutrient but, in excess, can lead to the formation of harmful free radicals. Therefore, a diverse set of cellular sensory and regulatory mechanisms is in place to control iron metabolism. Iron regulatory proteins (IRPs) are central to the cell's protective system, where they post-transcriptionally regulate other proteins responsible for cellular iron homeostasis. IRPs achieve this control by binding to iron-responsive elements (IREs), ~30-nucleotide-long stem–loops in the 5′ or 3′ untranslated regions of the corresponding messenger RNAs (mRNAs). IRPs do not possess common RNA binding motifs but still recognize and bind a variety of IRE stem–loops with picomolar affinity. The characteristic secondary structure adopted by IRP-bound IREs presents two separate regions for recognition: a terminal loop and a mid-stem bulge [1,2]. The five conserved nucleotides CAGUG of each IRE sequence (nucleotides 14–18 in our numbering) form the terminal pseudotriloop of the structure, with the central AGU triplet at the apex. The other important IRE feature is the conserved C8 bulge in the middle of the stem. The C8 hinge region forms multiple interactions when bound to IRP1. The IRE stem is divided into the upper helix between the C8 bulge and the terminal loop and the lower helix below the hinge.

Two IRPs are known: IRP1 and IRP2. They are highly homologous (~60% identity) and have similar overall affinities for IREs [3,4] but with distinct IRE recognition abilities [5–7]. The two IRPs are conserved in 15 of the 22 amino acids responsible for IRE binding. The variations may contribute to the differences in IRE recognition by these two proteins. During excess cellular iron levels, IRP1 becomes a cytosolic (c-) aconitase after acquiring a [4Fe–4S] cluster and looses RNA binding ability [8], while IRP2 undergoes degradation [9]. The unliganded apo-form of IRP1 precedes either functional form [8,10]. Apo-IRP1 undergoes proteasomal degradation when iron–sulfur cluster synthesis is defective, but with lower efficiency as compared to IRP2 [11].

IRP1 employs two known sites for IRE binding: the terminal loop-binding cavity and the pocket for the bulged C8 [1,2]. Each site involves all types of protein:RNA interactions, with hydrogen bonding being prominent. While hydrogen bonds do not constitute the strongest interactions between protein and RNA, they are responsible for binding specificity [12]. Early mutagenic studies of IRP1 provided insights regarding IRP:IRE interactions and importantly demonstrated the overlap of amino acids involved in RNA binding and aconitase active-site formation [13–19]. In the recent crystal structures of IRP1:IRE complexes, we identified many of the contacts for IRP1:IRE binding [1,2]. In this study, we focus on the five IRP1 residues—Arg269, Ser371, Lys379, Ser681, and Asn685—thought to determine the specificity of binding (Fig. 1) and investigate their contributions to complex stability and aconitase activity through site-specific mutagenesis of each residue.

Results

Rationale for construction of IRP1 mutants

In order to gain insight into the contribution of the five base-specific bonds to overall affinity and specificity of IRP1:IRE interaction, as well as to begin understanding the contribution of the individual binding interfaces to affinity of interaction, we mutated each of the base-specific contact residues to eliminate hydrogen bonding with the RNA base. Three mutations were made in the terminal loop-binding cavity. First, mutation of Arg269 to alanine

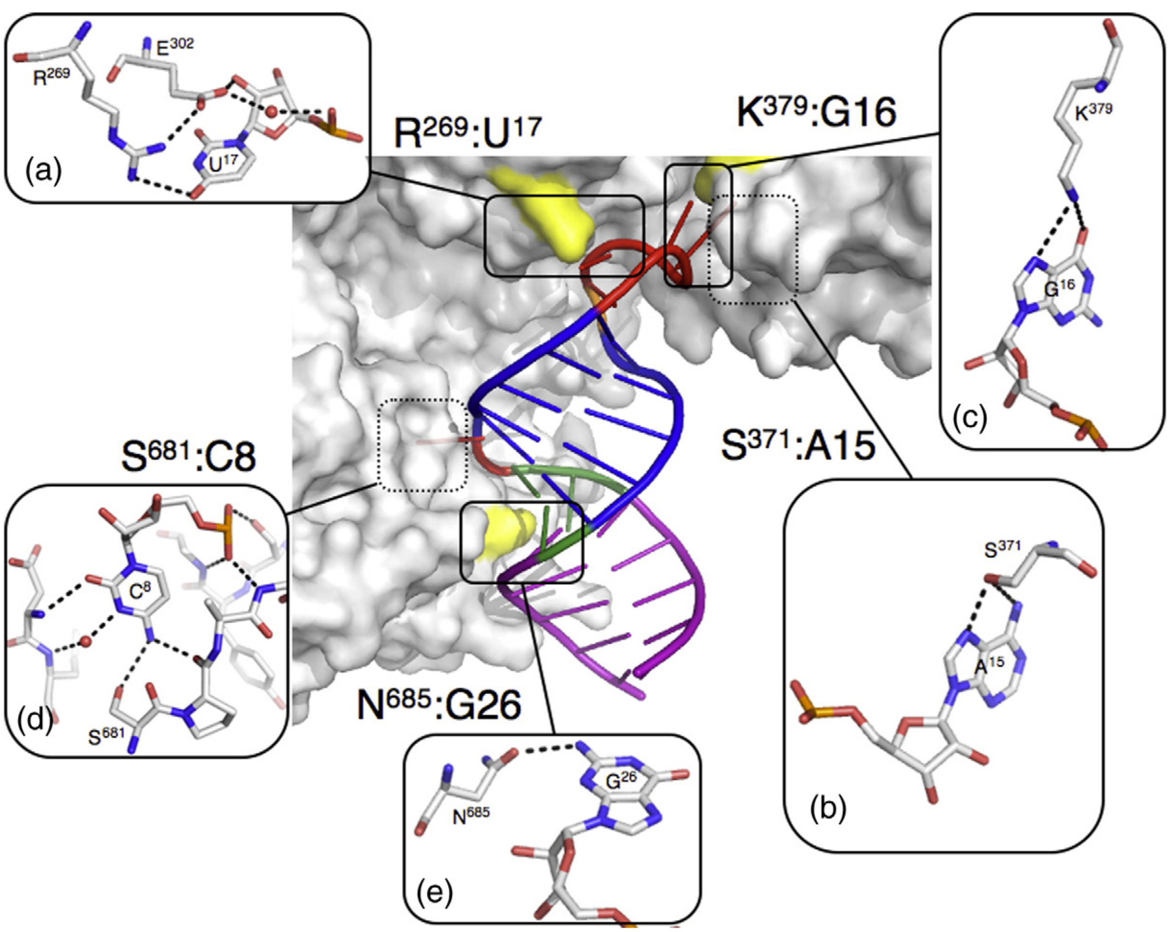

Fig. 1. The five IRP1 residues that form base-specific hydrogen bonds to the IRE RNA in the IRP1:IRE complexes. The IRE (cartoon) is shown as bound to the IRP1 protein (solvent-accessible surface). The amino acids Arg269, Lys379, and Asn685 are visible (yellow), while Ser371 and Ser681 are hidden from view. Details of the five base-specific contacts are shown by insets. Note that these residues are different from the four aconitase active-site arginines (Arg536, Arg541, Arg699, and Arg780) previously studied based on homology modeling [14–16].

should completely eliminate the hydrogen bond between the guanidinium group and O4 of U17 (Fig. 1a). Second, Ser371 was mutated to alanine and to aspartate: S371A should remove the bond between the hydroxyl of Ser371 and the N6 amino group of A15 (Fig. 1b), while the S371D substitution adds charge, bulk, and potential for steric clash in the loop-binding cavity. Third, Lys379 was mutated to asparagine and arginine to eliminate or alter the bond to O6 and N7 of G16 of the terminal loop (Fig. 1c).

In the C8 binding pocket, Ser681 was changed to alanine, which is expected to eliminate bonding of its hydroxyl with N4 of the C8 base (Fig. 1d). Moreover, Asn685, which was observed to form a base-specific hydrogen bond with N2 of the G26 base in the minor groove of the lower helix of ferritin IREs (Fig. 1e), was mutated to alanine and serine, which lack the capacity or are too short to make such a bond to the IRE.

Translational repression by IRP1 mutants

As a first step toward understanding the importance of each residue for IRP1 function, each mutant IRP1 was evaluated for ability to repress translation of an IRE-containing reporter mRNA in yeast as an initial interrogation of IRE-binding function. A chimeric IRE-luciferase gene under the transcriptional direction of the yeast ADH1 promoter served as the reporter and was integrated into the genome, creating strain AS4742 (see Experimental Procedures). Expression of wild-type IRP1 in AS4742 reduced luciferase expression by approximately 70% relative to the strain lacking any IRP1 (Fig. 2). Expression of each of the IRP1 mutants in this strain caused reduction in luciferase level, suggesting that each mutant protein retained some ability to bind IRE and repress translation of the IRE-luciferase mRNA. A similar level of repression of luciferase to that seen with wild-type IRP1 was observed upon expression of the R269A, K379R, N685A, and N685S IRP1 mutants, indicating comparable translational repression ability under the conditions used. The other IRP1 mutants (S371A, S371D, K379N, and S681A) were noticeably poorer at repression of luciferase in this system (Fig. 2). Importantly, there were comparable levels of wild type and each of the mutant IRP1 proteins in these yeast, indicating that the differential repression seen was most likely due to differential IRE binding ability of the IRP1 mutants.

IRE binding and K_d determinations for IRP1 mutants

To have a more quantitative analysis of IRE binding by these IRP1 mutant proteins, we used nitrocellulose filter-binding assays to determine dissociation constants (K_d) of the IRP1:IRE interactions [20,21]. Representative binding curves for the wild-type and IRP1 mutants are shown in Supplemental Fig. 1. The K_d for the complex of ferritin L IRE with wild-type IRP1 was measured at 17.6 ± 4.6 pM, which is in agreement with earlier published observations [20]. The K_d values for the N685A and N685S IRP1 mutants were equivalent to that of wild-type IRP1 (Table 1), indicating that Asn685 contributes little to the overall affinity of IRP1 interaction with human ferritin L IRE. The remaining IRP1 mutants fall into two categories based on the effect of the change on IRE binding affinity. Category 1, which includes the R269A, S371A, and K379R mutants, showed a decrease in IRE binding affinity around 10-fold (Table 1). Category 2, which includes the S371D, K379N, and S681A mutants, showed more than a 100-fold decrease in IRE binding affinity (Table 1). Binding of each of the category 2 mutants with human L-ferritin IRE was weak, increasing the uncertainty in the K_d values obtained with the nitrocellulose filter-binding assays. A significantly lower binding affinity for these IRP1 mutations was also suggested by the weaker translational repression observed in the yeast system (Fig. 2 and Supplemental Fig. 2). Thus, each of these mutations in IRP1 had a greater effect on IRE binding than would be predicted from simply a loss of a single hydrogen bond, and non-additive effects appear to be in play.

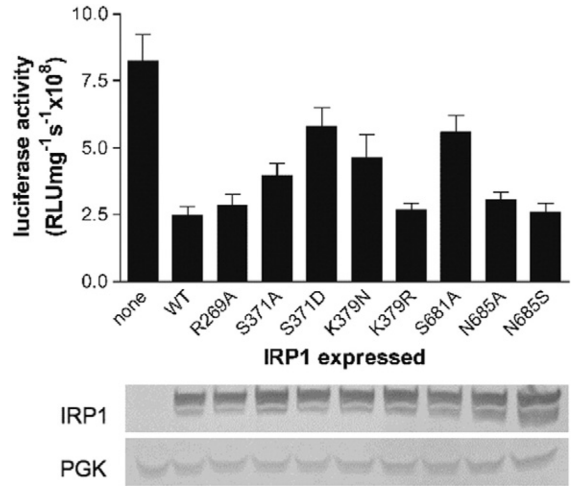

Fig. 2. Effect of IRP1 mutations on IRP-dependent translational repression. Luciferase activity measured in extracts of yeast strain AS4742 expressing the indicated IRP1. Cells were grown on SD-His-Ura synthetic media and harvested at logarithmic growth. The means and standard deviations of six independent experiments are shown. Luciferase activity is activity per total protein of extract. IRP1 expression levels were determined using immunoblotting with an antibody to a C-Myc epitope tag. Antibodies to PGK protein, one of the cell extract components, were used to monitor equal loading of extracts. Shown is one preparation out of six.

Table 1. K_d and K_{rel} values of WT and mutant IRP1 for ferritin L IRE

IRP1 expressed	K_d (pM) ± SD	K_{rel}
WT	17.6 ± 5	1.0
R269A	141. ± 49	8.0
S371A	212. ± 21	12.0
S371D	2400. ± 1200	>100
K379N	2900. ± 1300	>100
K379R	164. ± 60	9.3
S681A	3500. ± 1200	>100
N685A	10.6 ± 3	0.6
N685S	17.7 ± 6	1.0

Intracellular aconitase function of IRP1 mutants

The IRP1 mutants were examined for the alternate activity as an aconitase to gain insight into whether the mutations had general effects on protein function. To test for intracellular aconitase function, we investigated the ability of each IRP1 mutant to rescue aconitase-deficient (*aco-1*) yeast from glutamate auxotrophy. Yeast lacking aconitase cannot synthesize glutamate due to an inability to generate α-ketoglutarate, a precursor for glutamate synthesis, *via* the Kreb's cycle [22]. IRP1 can provide c-aconitase activity and restore glutamate prototrophy and growth of *aco1* yeast on glutamate-free media [23]. Each IRP1 mutant was transformed into the aconitase-deficient 0615d strain, and the resulting transformants were tested for growth on glutamate-free agar media (Fig. 3). All of the IRP1 mutants supported growth of this strain on glutamate-free media, although there were differences in the strength of growth. This indicated that each mutant was a functional aconitase within the yeast cell.

The aconitase activity from the IRP1 mutants was also examined in extracts of these yeasts. Activity was detected for all of the IRP1 mutants, although like growth, aconitase activity was variable (Fig. 4). In fact, growth rate in liquid glutamate-free media (Supplemental Fig. 3) correlated quite well with aconitase activity detected for IRP1 mutants (Fig. 5).

Reconstitution of aconitase activity in IRP1 mutants

To determine the effect of these IRP1 mutations on efficiency of aconitase function, we subjected each mutant protein in crude yeast extract to conditions for chemical FeS cluster reconstitution followed by analysis of aconitase activity [24]. Reconstitution of wild-type IRP1 under these conditions resulted in complete recovery of wild-type aconitase activity, at approximately 33 U/mg IRP1, which is in good agreement with published data for recovered wild-type activity [6] (Fig. 6). Cluster reconstitution of each of the IRP1 mutants restored significant aconitase activity as well (Fig. 6). Interestingly, the R269A, S371A, N685A, and N685S IRP1 mutants gave more than 2-fold higher aconitase specific activity than wild type, suggesting that these mutations might actually increase enzyme efficiency. The aconitase specific activity obtained for the K379N mutant was equivalent to wild-type protein, while the S371D, K379R, and S681A mutants gave a slightly reduced specific activity. However, it is important to note that the aconitase specific activity for these IRP1 mutants was within 2-fold of wild-type activity, whereas the negative effect on IRE binding of all but the Asn685 mutations was significantly greater.

Discussion

The highly specific binding of IREs by IRP1 occurs through two binding interfaces that combine to give one of the tightest protein:nucleic acid interactions in nature. Approximately two dozen hydrogen bonds identified in the crystal structure of the IRP1:ferritin IRE complex and distributed between the two binding interfaces support this interaction, but only five of the putative bonds are sequence specific. Here, through site-specific mutagenesis and functional analysis of mutant proteins, we show that mutation of four of the five amino acid residues—Arg269, Ser371, Lys379, and Ser681—significantly impaired interaction of IRP1 with ferritin IRE, confirming the importance of these bonds for IRP1:IRE recognition. Mutation at these sites caused reduction in binding affinity that ranged from 8-fold to more than 100-fold (Table 1). Thus, each of these contacts likely plays an important role in the specificity of the IRP1:IRE interaction, as well as to the overall affinity.

Mutation at the fifth site, Asn685, did not alter ferritin IRE binding (Table 1). We previously observed that Asn685 forms a base-specific hydrogen bond with G26 atom N2 in the IRP1:ferritin H IRE complex, made possible by the wobble base-pair G26:U5 that is unique to ferritin IREs [1]. However, the geometry of this putative bond was not optimal (Fig. 1e). The results reported here indicate that a bond between Asn685 and G26, if it exists, does not contribute to the overall affinity of IRP1:ferritin IRE interaction (Table 1). This is consistent with the observations of Goforth *et al.* that mutation of ferritin IRE to eliminate this contact had little to no effect on protein:RNA binding [7].

Of the two interfaces used for the IRP1:IRE interactions—the IRP1 cavity with terminal loop *versus* the IRP1 pocket with C8 bulge—the former is more complex, with greater size and more extensive bonding. Three amino acid–nucleotide base-specific contacts are confined to the terminal loop-binding cavity: Arg269 with U17, Ser371 with A15, and Lys379 with G16 (Fig. 1a–c). In the IRP1: IRE complexes, Arg269 interacts with U17, the

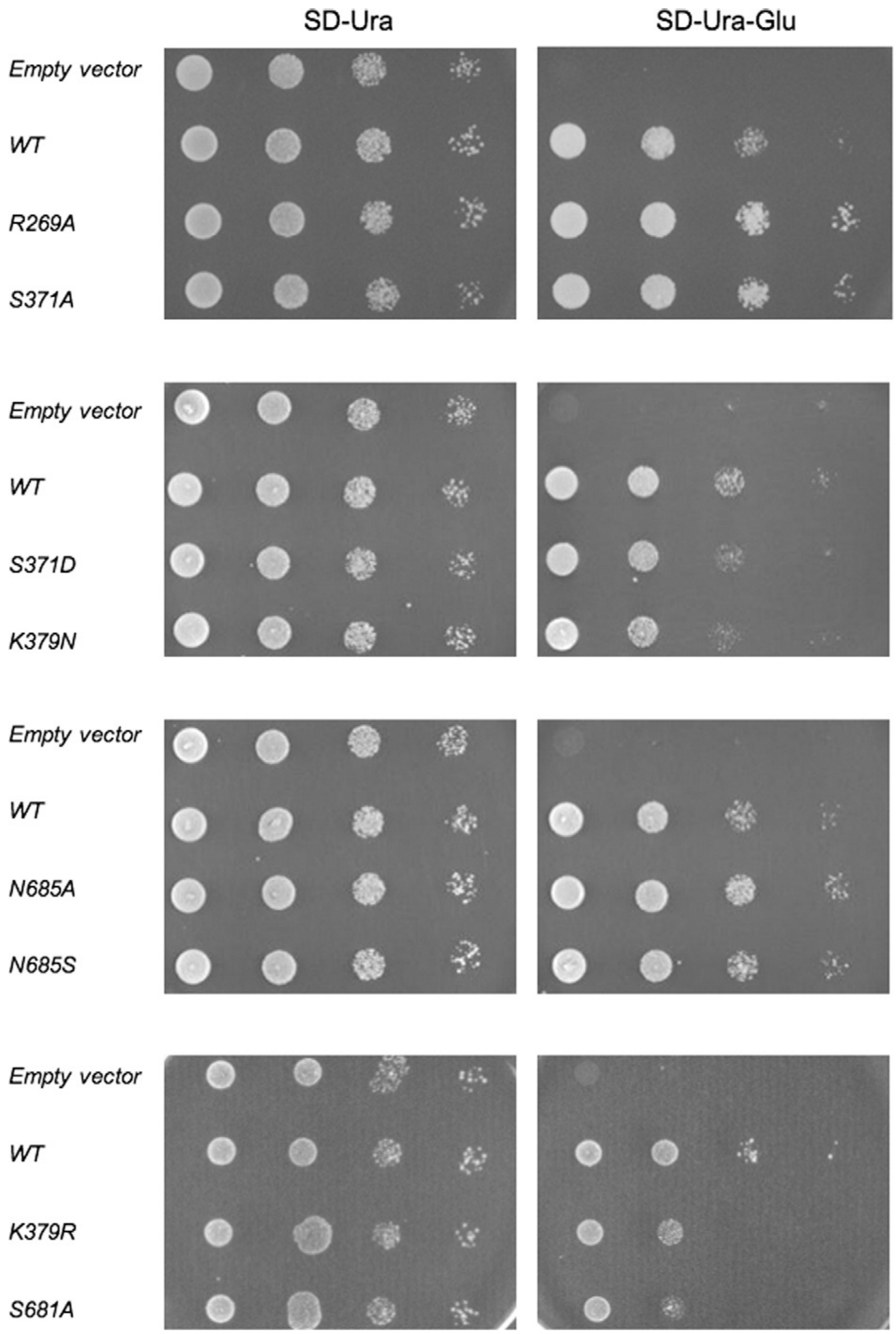

Fig. 3. Ability of IRP1 mutants to rescue *aco-1* yeast strains from glutamate auxotrophy. Strain 0651d expressing the indicated IRP1 was grown to mid-logarithmic phase in SD-Ura, washed twice with sterile H_2O, and then spotted as 10-μl aliquots of serial dilutions containing from 10^2 to 10^5 cells on SD-Ura with or without glutamate as indicated.

topmost stacked base of the IRE stem, where its guanidinium group has a hydrogen bond to the exposed O4 of the uracil base (Fig. 1a). The Arg269A substitution eliminated this base-specific interaction and reduced IRP1:IRE binding by 8-fold (Table 1). The magnitude of the reduction seems large given that the Arg269–U17 interaction is solvent accessible and that the side chain has access to other conformations. Probably, the additional bond to the neighboring (and also IRP invariant) Glu302 carboxyl stabilizes this interaction, while the stacking of Glu302 on top of U17 also contributes to the high IRP:IRE affinity. U17 is not invariant among naturally occurring IRE sequences.

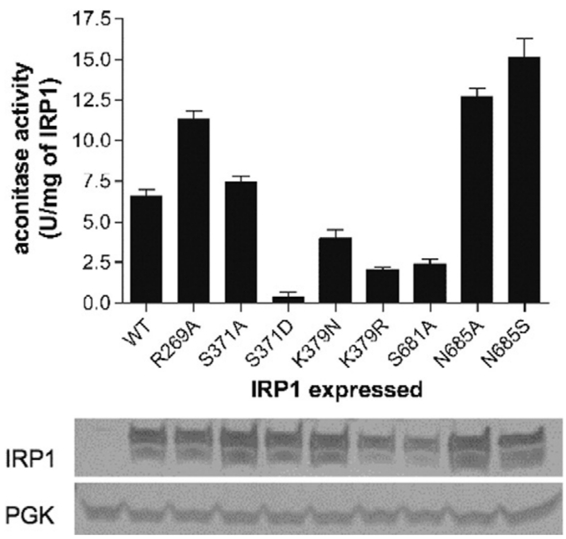

Fig. 4. Aconitase activity of IRP1 mutants. Aconitase specific activity of the indicated IRP1 mutants in crude yeast cytoplasmic extracts. Error bars indicate standard deviations for three experiments. IRP1 expression levels were determined using immunoblotting with an antibody to a C-Myc epitope tag. Antibodies to PGK protein, one of the cell extract components, were used to monitor equal loading of extracts. Shown is one preparation out of five.

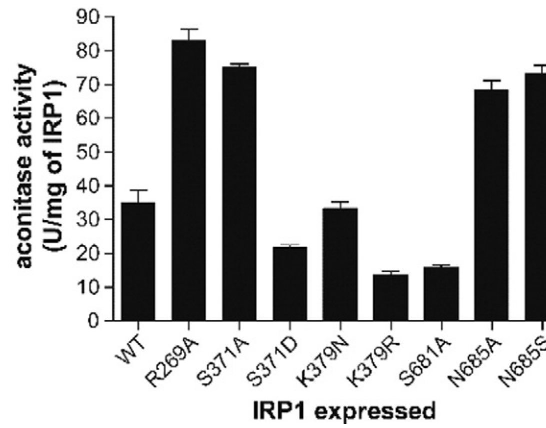

Fig. 6. Aconitase activity of IRP1 mutants after iron–sulfur cluster reconstitution. Error bars indicate standard deviations for three experiments.

For example, it is A17 in the 3′ IRE that regulates translation of MRCKα, a serine/threonine kinase involved in cytoskeletal reorganization [25]. The CAGAG terminal loop sequence of the MRCKα IRE was originally reported to have the same or possibly higher binding affinity as the wild-type CAGUG [25]. Simple model building shows that the terminal loop and binding cavity can accommodate the uridine-to-adenine switch with no clashes. However, the introduced extracyclic amine (N6) would be closest to the guanidinium of Arg269, which, contrary to above, should reduce the bonding potential. This discrepancy is not understood, but perhaps other elements of the IRP1:MRCKα IRE interaction can compensate. In addition to the U17A variant in the MRCKα IRE, there are U17G and U17C substitutions in the TfR1 A IREs from two species of fish and chicken [26]. If TfR1 A IREs are truly functional [27], then sequence variety at this position in the IRE family must be accommodated by other means.

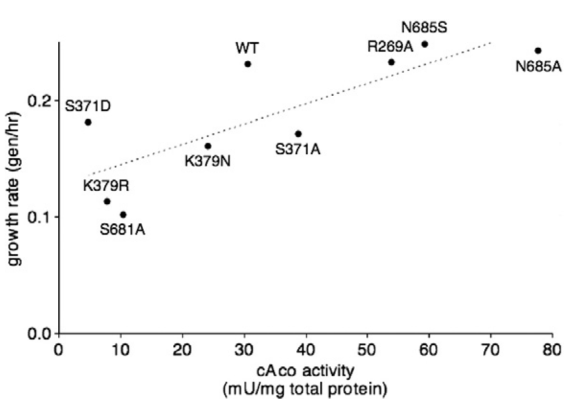

Fig. 5. Correlation of aconitase-dependent growth rate with aconitase activity for wild-type and mutated IRP1. R^2 = 0.64. Growth rates were calculated from the growth curves shown in Supplemental Fig. 3.

The Ser371 hydroxyl has a hydrogen bond with the N6 amino group of the fully extended A15 of the IRE terminal loop in the IRP1:IRE complexes, and possibly with N7 (Fig. 1b). Conservation of the Ser371-to-A15 interaction appears absolute: Ser371 is invariant in all IRPs investigated, and there are no known normally functioning IRE variants at position 15 of the apical loop. The S371A substitution in IRP1 eliminates the serine hydroxyl and decreases the binding strength 12-fold, while an aspartate substitution (S371D) has a stronger inhibitory effect on binding affinity, decreasing it by more than 100-fold (Table 1). These two mutations thus demonstrate both the importance of the hydrogen bonds and the consequence of charge and steric clash at that site. For the S371D mutation, there is simply no space to accommodate the added aspartate charge and bulk; thus, A15 would not be able to fully extend into the cavity it normally occupies in the IRP1:IRE complex. It is likely that the charge change from the S371D substitution also disrupts the neighboring interactions of Lys379 with G16 (see below). There are two spontaneous mutations at position 15 of human ferritin IREs that present different pathophysiologies: A15G and A15U [28]. In the first case, an A15G transition in ferritin L IRE is responsible for the heritable hypoferritinemia cataract syndrome (HHCS) mutation known as Paris 1 [29]. The A15G mutation reduced IRP1 affinity by ~200-fold as measured in IRE competition experiments [4]. An amino-to-oxo switch at C6 of the purine eliminates the only hydrogen donor to Ser371, similar in effect to the S371A IRP1 substitution, but the ~200-fold decrease in IRE affinity is roughly an order of magnitude worse than the effect of the S371A substitution measured here. The 2-amino group of A15G may also contribute to the decrease. In the second case, an A15U substitution in ferritin H causes an iron overload disorder, which is heritable as an autosomal dominant trait [30]. It was reported to cause a 2-fold higher affinity for IRP1. Simple modeling of the A15U transversion (assuming the same stem–loop folding and stability) does not suggest an increase in affinity between the introduced O4 carbonyl and the S371 hydroxyl.

Lys379 of IRP1 binds to O6 and N7 of G16 in the terminal loop-binding cavity in the IRP1:IRE complexes (Fig. 1c). Our results with the K379R mutant IRP1 showed a 9-fold decrease in the binding strength to ferritin L IRE (Table 1). The K379R substitution (which occurs naturally at the equivalent position in IRP2) preserves the positive charge of the residue but introduces the larger guanidinium group, possibly creating strain on the interactions in the terminal loop-binding cavity. This difference between IRPs may contribute to the observed higher tolerance for variation at IRE position 17 for binding by IRP2 [31]. The K379N substitution shows even greater weakening (>100-fold) of the IRP1:IRE interaction. Elimination of the positive charge on residue 379 may affect binding of the entire terminal loop, possibly by reducing the ability of IRP1 to stabilize the IRE conformation that promotes high-affinity interaction. An equivalent effect is seen with the introduction of the negative charge in the S371D substitution discussed above. As for spontaneous, disease-causing HHCS mutations at position 16 of IREs, the G16C substitution of the ferritin L IRE known as Verona [32] causes the largest loss in IRP affinity of all [4]. Clearly, the introduction of the C16 N4 amino group would completely eliminate attractive interaction with the Lys379 side chain.

The C8 bulge region may be the simpler of the two IRP:IRE recognition interfaces because it involves just one unpaired nucleotide. The pocket for C8 is lined with many hydrogen bonding groups, and the cytosine base forms hydrogen bonds with four of them (Fig. 1d). However, three are through backbone atoms and/or solvent: only Ser681 provides a functional side chain, where the γ hydroxyl makes a hydrogen bond with N4 of the deeply buried C8 base. Elimination of that interaction by a S681A substitution decreases the IRP1:IRE binding affinity by more than 100-fold, an effect obviously far greater than removal of a single hydrogen bond. Ser681 is absolutely conserved in all IRP1 and IRP2 sequences. The restricted volume of the pocket and complementarity to C8 might dictate that any substitution at position 8 would be unfavorable. Indeed, two independent types of HHCS are caused by the naturally occurring mutations C8U and C8A in the human ferritin L IRE [33,34] (their IRP binding strengths have not been determined). Oddly however, a C-to-G substitution at position 8 is permissible in the IREs of sand worms, sea squirts, crayfish, and shrimp [26] (their functionalities are yet to be demonstrated). It is tempting to assume that their IRP pockets evolved in parallel with their IREs to accommodate the larger purine, but a homology modeling experiment with the crayfish IRP1 sequence (*Pacifastacus leniusculus*; 69% identity with *Homo sapiens*) revealed total conservation in and around the binding pocket (K.W.V., unpublished results).

This is the first study to functionally define the IRP1 residues that form specific hydrogen bonds to the IRE bases, analogous to the studies of the FeS cluster-binding cysteine residues necessary for the aconitase function [13,15]. Comparison of the crystal structures of the IRP1:IRE complexes with c-aconitase shows extensive overlap between the IRE binding and aconitase active sites, with several amino acid residues playing important roles in both [1,35]. However, none of the residues that make sequence-specific bonds with IRE are aconitase active-site residues (Supplemental Fig. 4). Analysis of aconitase function of mutant IRP1 by yeast growth and in extracts showed all of the IRP1 mutants to be functional aconitases (Figs. 3–6). Upon FeS cluster reconstitution, the mutant c-aconitases gave specific activities within 2-fold of wild type (Fig. 6). The positive effects of some mutations on aconitase activity were surprising, showing that the bifunctionalities of IRP1 are more integrated than expected. This is despite the fact that the residues in this study are more than 15 Å from the c-aconitase FeS cluster (Supplemental Figs. 4 and 5).

It is not yet possible to predict whether a particular aconitase has dual IRE binding and aconitase functions similar to those of mammals or functions only as an aconitase. The IRP1 residues that make contact with the IRE are mainly conserved in the IRP/AcnA branch of the aconitase superfamily. One exception is Lys379, which is primarily an arginine in non-IRE-binding c-aconitases. As discussed above, the equivalent residue is arginine in all known IRP2s as well. This suggests that amino acid residue identity, while important, is not the sole determinant of function as an IRE-binding protein. Nonetheless, Lys379 and Ser681 appear to be particularly crucial to IRE binding in that mutations of these residues cause the greatest impairment of binding. Both G16 and C8 of the IRE, the respective bonding sites for Lys379 and Ser681, are fully extended and accommodated by the protein in the complex [1,2]. It is intriguing to think that the key features selected in the evolution of this high-affinity protein:RNA regulatory system were the contacts that stabilized the extended conformation of the conserved nucleotides of the IRE, providing a level of selectivity that would eventually mediate control of cellular iron metabolism.

Experimental Procedures

IRP1 mutagenesis and expression in yeast

Site-specific mutagenesis of rabbit IRP1 was performed using the Stratagene QuikChange II Site-Directed Mutagenesis Kit following the manufacturer's recommended procedure. An identical set of mutations was engineered in vectors designed to express the protein with an N-terminal 6-His tag for protein purification or with a C-terminal myc-epitope tag for all other uses [36,37]. All mutations were verified by DNA sequencing. Overexpression of wild-type and mutant IRP1 and purification from yeast was performed as described previously [36]. To assess aconitase function, we expressed IRP1 mutants in the aconitase-deficient 0615d *Saccharomyces cerevisiae* strain (*MAT*a, *ura3-52*, *trp1-Δ63*, *his3-Δ200*, *aco1-1*, *ade2*, *IDP2*^{up}) [23,37]. To assess the translational repression function of mutant IRP1 in yeast, we constructed the strain AS4742 by integrating an IRE-luciferase reporter gene in which the firefly luciferase open reading frame was fused to the human L-chain IRE sequence under transcriptional direction of a minimal ADH1 promoter [23] into the yeast genome at the *HIS3* locus of strain BY4742 (Open Biosystems). All yeast transformations were performed using the lithium acetate method [38]. Yeast were routinely grown at 30 °C in synthetic dropout (SD) media supplemented with 2% dextrose and lacking the appropriate nutrient for selection and maintenance of plasmids [39]. For testing aconitase function of IRP1 mutants in yeast, growth analysis was performed in SD lacking glutamate [37].

Yeast cytoplasmic extract preparation and enzyme assays

Preparation of yeast cytoplasmic extracts, determination of total extract protein, protein immunoblot, and enzyme assays were performed as described elsewhere [23,37]. Standard aconitase activity assay conditions consisted of 10.0 mM Tris–HCl (pH 8.0) and 2.0 mM D/L-trisodium isocitrate. FeS cluster reconstitution was performed chemically by incubating yeast extracts containing IRP1 with 0.5 mM $Fe(NH_4)_2(SO_4)_2$, 0.5 mM Na_2S, and 5 mM DTT for 1 h at room temperature. Yeast extracts for IRP1 expression analysis were prepared using the post-alkaline method [40]. Western blot images were quantified using Alpha Imager software and statistically processed using GraphPad Prism software (GraphPad Software, Inc.).

IRP1:IRE affinity measurement

The affinity of each of the IRP1 mutant proteins for human ferritin L IRE was determined using purified proteins and nitrocellulose filter-binding assay [20]. His-tagged IRP1 was expressed and purified using a Ni affinity column as described previously [36]. The purity of each protein preparation was >95% as determined by SDS-PAGE. Single-use aliquots in 20 mM Tris (pH 7.4), 100 mM KCl, 10% glycerol, and 5 mM DTT were stored at −80 °C at concentrations from 20.6 to 42.9 μM. [^{32}P]human L-ferritin IRE probe was prepared from pTZM1 and used in nitrocellulose filter-binding assays as described by Swenson *et al.* [20]. The complex dissociation constant for each IRP1 variant was determined from RNA saturation curves (1.3 pM to 15 nM) performed under equilibrium conditions, where increasing amounts of radioactively labeled IRE transcripts were added to constant amounts of protein. Standard binding conditions consisted of 50 mM Tris–HCl (pH 7.5), 40 mM KCl, 3 mM $MgCl_2$, 1 mM DTT, 20 μg/ml bovine serum albumin, and 66 μg/ml *Escherichia coli* tRNA. Reactions were performed in triplicate at 37 °C for 20 min and then passed through 24-mm nitrocellulose filters (Millipore-HAWP), which had been pre-equilibrated with binding buffer. Filters were immediately washed with five volumes of ice-cold binding buffer. Average time of washing was 4 s. Filters were dried at 80 °C for 30 min and bound radioactivity was measured by liquid scintillation. Data analysis and curve fitting were performed using GraphPad Prism (GraphPad Software, Inc.).

Acknowledgements

This work was supported by National Institutes of Health grant GM-71504 to K.W.V.

Supplementary Data

Supplementary data to this article can be found online at http://dx.doi.org/10.1016/j.jmb.2013.06.023.

Received 27 December 2012;
Received in revised form 31 May 2013;
Accepted 17 June 2013
Available online 25 June 2013

Keywords:
iron homeostasis;
iron regulatory protein;
bifunctionality;
RNA binding

Abbreviations used:

IRP, iron regulatory protein; IRE, iron-responsive element; HHCS, heritable hypoferritinemia cataract syndrome.

References

[1] Walden WE, Selezneva A, Dupuy J, Volbeda A, Fontecilla-Camps JC, Theil E, et al. Structure of dual function iron regulatory protein 1 complexed with ferritin IRE-RNA. Science 2006;314:1903–9.

[2] Walden WE, Selezneva A, Volz K. Accommodating variety in iron-responsive elements: crystal structure of transferrin receptor 1 B IRE bound to iron regulatory protein 1. FEBS Lett 2012;314:32–5.

[3] Kim HY, Klausner RD, Rouault TA. Translational repressor activity is equivalent and is quantitatively predicted by *in vitro* RNA binding for two iron-responsive element binding proteins, IRP1 and IRP2. J Biol Chem 1995;270:4983–6.

[4] Allerson CR, Cazzola M, Rouault TA. Clinical severity and thermodynamic effects of iron-responsive element mutations in hereditary hyperferritinemia-cataract syndrome. J Biol Chem 1999;274:26439–47.

[5] Henderson BR, Menotti E, Bonnard C, Kühn LC. Optimal sequence and structure of iron-responsive elements: selection of RNA stem–loops with high affinity for iron regulatory factor. J Biol Chem 1994;269:17481–9.

[6] Theil EC, Eisenstein RS. Iron regulatory proteins and iso-iron-responsive elements (iso-IREs). J Biol Chem 2000;275:40659–62.

[7] Goforth JB, Anderson S, Nizzi CP, Eisenstein RS. Multiple determinants within iron-responsive elements dictate iron regulatory protein binding and regulatory hierarchy. RNA 2010;16:154–69.

[8] Haile DJ, Rouault TA, Harford JB, Kennedy MC, Blondin GA, Beinert H, et al. Cellular regulation of the iron-responsive element binding protein: disassembly of the cubane iron-sulfur cluster results in high-affinity RNA binding. Proc Natl Acad Sci USA 1992;89:11735–9.

[9] Guo B, Phillips JD, Yu Y, Leibold EA. Iron regulates the intracellular degradation of iron regulatory protein 2 by the proteasome. J Biol Chem 1995;270:21645–51.

[10] Shand O, Volz KW. The solution structure of apo-iron regulatory protein 1. Gene 2013;524:341–6.

[11] Wang J, Fillebeen C, Chen G, Biederbick A, Lill R, Pantopoulos K. Iron-dependent degradation of apo-IRP1 by the ubiquitin-proteasome pathway. Mol Cell Biol 2007;27:2423–30.

[12] Morozova N, Allers J, Myers J, Shamoo Y. Protein–RNA interactions: exploring binding patterns with a three-dimensional superposition analysis of high-resolution structures. Bioinformatics 2006;22:2746–52.

[13] Philpott CC, Haile D, Rouault TA, Klausner RD. Modification of a free Fe-S cluster cysteine residue in the active iron-responsive element-binding protein prevents RNA binding. J Biol Chem 1993;268:17655–8.

[14] Philpott CC, Klausner RD, Rouault TA. The bi-functional iron-responsive element binding protein/cytosolic aconitase: the role of active site residues in ligand binding and regulation. Proc Natl Acad Sci USA 1994;91:7321–5.

[15] Hirling H, Henderson BR, Kühn LC. Mutational analysis of the [4Fe–4S]-cluster converting regulatory factor from its RNA-binding form to cytoplasmic aconitase. EMBO J 1994;13:453–61.

[16] Butt J, Kim H-Y, Basilion JP, Cohen S, Iwai K, Philpott CC, et al. Differences in the RNA binding sites of iron regulatory proteins and potential target diversity. Proc Natl Acad Sci USA 1996;93:4345–9.

[17] Gegout V, Schlegl J, Schläger B, Hentze MW, Reinbolt J, Ehresmann B, et al. Ligand-induced structural alterations in human iron regulatory protein-1 revealed by protein footprinting. J Biol Chem 1999;274:15052–8.

[18] Kaldy P, Menotti E, Moret R, Kühn LC. Identification of RNA-binding surfaces in iron regulatory protein-1. EMBO J 1999;18:6073–83.

[19] Pitula JS, Deck KM, Clarke SL, Anderson SA, Vasanthakumar A, Eisenstein RS. Selective inhibition of the citrate-to-isocitrate reaction of cytosolic aconitase by phosphomimetic mutation of serine-711. Proc Natl Acad Sci USA 2004;101:10907–12.

[20] Swenson GR, Patino M, Beck M, Gaffield L, Walden WE. Characteristics of the interaction of the ferritin repressor protein with the iron responsive element. Biol Met 1991;4:48–55.

[21] Ryder SP, Recht MI, Williamson JR. Quantitative analysis of protein–RNA interactions by gel mobility shift. Methods Mol Biol 2008;488:99–115.

[22] Ogur M, Coker L, Ogur S. Glutamate auxotrophs in *Saccharomyces*. I. The biochemical lesion in the glt_1 mutants. Biochem Biophys Res Commun 1964;14:193–7.

[23] Narahari J, Ma R, Wang M, Walden WE. The aconitase function of iron regulatory protein 1: genetic studies in yeast implicate its role in iron-mediated redox regulation. J Biol Chem 2000;275:16227–34.

[24] Kennedy MC, Mende-Mueller L, Blondin GA, Beinert H. Purification and characterization of cytosolic aconitase from beef liver and its relationship to the iron-responsive element binding protein. Proc Natl Acad Sci USA 1992;89:11730–4.

[25] Cmejla R, Petrak J, Cmejlova J. A novel iron responsive element in the 3′ UTR of the human MRCKα. Biochem Biophys Res Commun 2006;341:158–66.

[26] Piccinelli P, Samuelsson T. Evolution of the iron-responsive element. RNA 2007;13:952–66.

[27] Casey JL, Koeller DM, Ramin VC, Klausner RD, Harford JB. Iron regulation of transferrin receptor mRNA levels requires iron-responsive elements and a rapid turnover determinant in the 3′ untranslated region of the mRNA. EMBO J 1989;8:3693–9.

[28] Cazzola M, Skoda RC. Translational pathophysiology: a novel molecular mechanism of human disease. Blood 2000;95:3280–8.

[29] Bonneau D, Winter-Fuseau I, Louiseau M-N. Bilateral cataract and high serum ferritin: a new dominant genetic disorder? J Med Genet 1995;32:778–9.

[30] Kato J, Fujikawa K, Kanda M, Fukuda N, Sasaki K, Takayama T, et al. A mutation, in the iron-responsive element of H ferritin mRNA, causing autosomal dominant iron overload. Am J Hum Genet 2001;69:191–7.

[31] Henderson BR, Menotti E, Kühn LC. Iron regulatory proteins 1 and 2 bind distinct sets of RNA target sequences. J Biol Chem 1996;271:4900–8.

[32] Girelli D, Corrocher R, Bisceglia L, Olivieri O, De Franceschi L, Zelante L, et al. Molecular basis for the recently described

hereditary hyperferritinemia-cataract syndrome: a mutation in the iron-responsive element of ferritin-L subunit gene (the “Verona mutation”). Blood 1995;86:4050–3.
[33] Balas A, Aviles MJ, Garcia-Sanchez F, Vicario JL, Cervera A. Description of a new mutation in the L-ferritin iron-responsive element associated with hereditary hyperferritinemia-cataract syndrome in a Spanish family. Blood 1999;93:4020–1.
[34] Giansily M, Beaumont C, Desveaux C, Hetet G, Schved JF, Aguilar-Martinez P. Denaturing gradient gel electrophoresis screening for mutations in the hereditary hyperferritinaemia cataract syndrome. Br J Haematol 2001;112:51–4.
[35] Volz K. The functional duality of iron regulatory protein 1. Curr Opin Struct Biol 2008;18:106–11.
[36] Selezneva AI, Cavigiolio G, Theil EC, Walden WE, Volz K. Crystallization and preliminary X-ray diffraction analysis of iron regulatory protein-1 in complex with ferritin IRE RNA. Acta Crystallogr Sect F Struct Biol Cryst Commun 2006;62:249–52.
[37] Brown NM, Anderson SA, Steffen DW, Carpenter TB, Kennedy MC, Walden WE, et al. Novel role of phosphorylation in 4Fe–4S cluster stability revealed by phosphomimetic mutations at serine 138 of iron regulatory protein 1. Proc Natl Acad Sci USA 1998;95:15235–40.
[38] Ito H, Fukuda Y, Murata K, Kimura A. Transformation of intact yeast cells treated with alkali ions. J Bacteriol 1983;153:163–8.
[39] Sherman F. Getting started with yeast. Methods Enzymol 1991;194:3–21.
[40] Kushnirov VV. Rapid and reliable protein extraction from yeast. Yeast 2000;16:857–60.